ACS Partner Journal

CHEM & BIO ENGINEERING

pubs.acs.org/ChemBioEng

Letter

Hydration/Dehydration Induced Reversible Transformation between a Porous Hydrogen-Bonded Organic Framework and a Nonporous Molecular Crystal for Highly Efficient Gas Dehydration

Published as part of Chem & Bio Engineering virtual special issue "Advanced Separation Materials and Processes".

Yao Wang, Xiyu Song, Guanglai Mo, Xiangyu Gao, Enyu Wu, Bin Li, Yunbo Bi,* and Peng Li*

Cite This: *Chem Bio Eng.* 2024, 1, 283−288

Read Online

ACCESS | Metrics & More | Article Recommendations | Supporting Information

ABSTRACT: Gas dehydration is a critical process in gas transportation and chemical reactions, yet traditional drying agents require an energy-intensive dehydration and regeneration step. Here, we present a nonporous molecular crystal called Melem that can be synthesized and scaled up through solid-state synthesis methods. Melem exhibits exceptional water selectivity in gas dehydration and can be reactivated under moderate conditions. According to the single-crystal structure and powder X-ray diffraction studies, a reversible structural transformation between Melem and its hydrated form, Melem−H_2O, induced by hydration/dehydration processes has been observed. Melem displays water adsorption properties with a maximum uptake of 11 mmol·g^{-1} at p/p_0 = 0.92 and 298 K. Additionally, Melem retained consistent water capture capacities after 5 adsorption−desorption cycles. The remarkable gas dehydration performance of Melem was confirmed by column breakthrough experiments, which achieved a separation factor of up to 654.

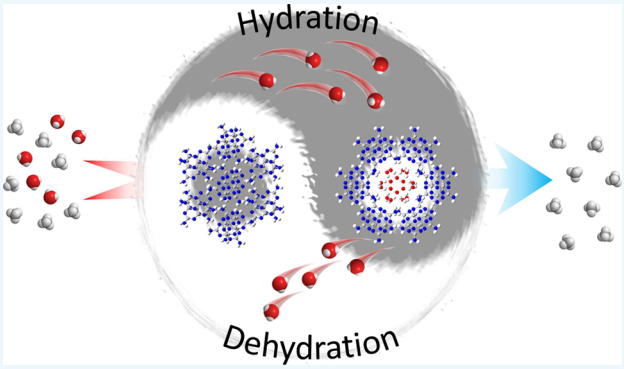

Water vapor is one of the main causes for pipeline corrosion and blockage during gas transportation.[1,2] The presence of water can significantly reduce the efficiency of chemical reactions, such as in methane dry reforming.[3] Gases are typically dried using solid desiccants such as zeolites 3A, 4A, and 13X.[4] These solid desiccants require heating to approximately 200 °C for activation. This process demands substantial energy and involves the risk of adsorbent pore collapse. In addition, commercial solid desiccants also exhibit a high affinity for CO_2, which makes them less efficient in drying gas streams containing CO_2. It is of utmost importance to discover a viable solution that effectively addresses all these challenges.

In recent years, porous materials such as metal−organic frameworks have gained extensive attention for separation applications, including gas drying.[5−10] Normally, factors such as the rigid pore environment, limited adsorption site density, and dynamic competition among various guest species hinder the potential of porous materials to enhance selectivity.[11−13] Hydrogen-bonded organic frameworks (HOFs), a class of porous materials constructed by weak noncovalent intermolecular interactions (hydrogen bonding and $\pi\cdots\pi$ stacking), have emerged rapidly as multifunctional materials for gas storage,[14,15] separation,[16−18] proton conduction,[19,20] sensing,[21−24] enzyme encapsulation,[25−27] antibacterial activity,[28,29] and applications over the past decade.[30−32] Due to the flexible and weak nature of hydrogen bonds, the original intermolecular interactions in HOFs may be disrupted or reorganized under specific driving forces, causing changes in the pore environments, adsorption sites, and pore size.[33,34] By taking advantage of the characteristics of hydrogen bonding, designing nonporous hydrogen-bonded molecular crystals that display pore-opening responses to particular guest molecules can markedly enhance their utility in molecular recognition and separations. Rahmani et al. found that nonporous TPBD allows for highly selective capture of *p*-xylene, undergoing a structure transformation from TPBD to TPBD-PX.[35] Molecular crystals with hydrophilic functional groups, such as amino

Published: March 12, 2024

and 2,4-diamino triazine (DAT) groups might be promising adsorbent materials for selective recognition and separation of water.[36−39]

In this study, we observed a reversible structural transformation process featuring pore opening/closing, induced by hydration/dehydration, which could be utilized for the specific recognition and adsorption of water during gas dehydration. We found that Melem, a nonporous molecular crystal composed of 1,3,3a^1,4,6,7,9-heptaazaphenalene-2,5,8-triamine, exhibited a unique pore-opening effect toward the water. The reversible structural framework transformation between the nonporous Melem and porous Melem−H_2O can be observed by single-crystal X-ray structures and powder X-ray diffraction (PXRD). The nonporous nature of Melem could avoid the influence of gases on H_2O adsorption properties. Melem exhibits a maximum adsorption capacity of approximately 11.0 mmol·g^{-1} for water, and its adsorption capacity remains unchanged after at least 5 consecutive adsorption−desorption cycles. Column breakthrough experiments have further established its gas dehydration performance. Additionally, Melem demonstrated good thermal stability and can be readily regenerated without compromising its performance, showcasing its promising practical applications in the field of gas dehydration.

The crude nonporous Melem was obtained using melamine as the precursor under 430 °C (Scheme 1).[39−41] After

Scheme 1. Schematic of the Synthesis of Melem and the Hydration/Dehydration-Induced Reversible Transformation Process[a]

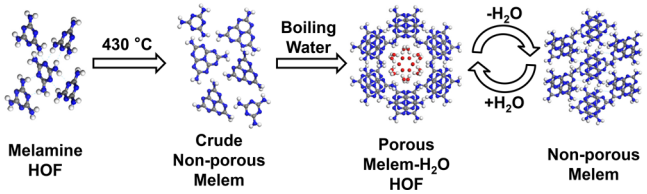

[a]The red, white, gray, and blue balls represent O, H, C, and N atoms, respectively.

removing the melamine by boiling water, the nonporous Melem rebuilds into Melem−H_2O by a hydrogen bond.[42,43] The Melem−H_2O could be returned to nonporous Melem by heating to remove the H_2O from the frameworks. The Melem was crystallized in a monoclinic system with the $P2_1/c$ space group, while the Melem−H_2O was crystallized in a trigonal system with the $R\bar{3}c$ space group. Melem was assembled by intermolecular hydrogen bonds and $\pi-\pi$ stacking between the inversion CN heterocyclic rings (Figure 1a−d). With the introduction of H_2O, the original intermolecular hydrogen bonds were broken, forming 1D channels with a diameter of 9.5 Å (Figure 1e,f). The O-positions obtained from the structure are shown schematically in Figure 1f and consist of a hexamer. Each water molecule establishes hydrogen bonds with two other water molecules and two Melem molecules, with one Melem molecule contributing an amino group and the other supplying nitrogen of the hexagonal nitrogen ring. The distance of the adjacent water oxygen atom was 3.3 Å in the range of characteristic H-bonding distance. The hexagonal channels with a diameter of 5.3 Å formed by water hexamer allowed further filling by H_2O molecules. The layer distance between Melem molecules decreased from 3.3 to 3.1 Å while maintaining the form of inverted stacking (Figure 1g,h).

The PXRD results demonstrated the phase change after water adsorption and desorption (Figure 2a). After heating and dehydration, the disappearance of the diffraction peaks at 2θ = 6.1 and 10.6° indicated that the frame of Melem−H_2O began to collapse. In addition, the diffraction peaks at 2θ = 24−28° become cluttered, suggesting a layer-to-layer rearrangement. The formation of new diffraction peaks at 2θ = 13.4, 25.8, and 26.2° demonstrated the formation of nonporous Melem. The diffraction peaks belonging to Melem−H_2O at 2θ = 6.1 and 10.6° would reappear after absorbing water or leaving them in moist air for a few days. The scanning electron microscopy (SEM) photographs revealed the topography changes of Melem−H_2O and Melem (Figure S1). Microcrystals of Melem−H_2O were observed to adopt a hexagonal prismatic shape, whereas Melem microcrystals maintained a rod-like morphology.

To assess the H_2O adsorption performance of Melem, we measured the water adsorption isotherms. Due to the Melem being in a nonporous phase at lower relative humidity (RH), its adsorption capacity for H_2O is relatively weak (Figure 2b). As the amount of H_2O adsorption increases, the pore channel gradually opens and the rate of H_2O adsorption increases rapidly. The inflection point occurred around 33% RH (4.58 mmol·g^{-1}), which corresponded to the state of one H_2O molecule per Melem (Figure 1f). It implies that the pore channel is fully open. The following adsorbed H_2O molecules further form intermolecular hydrogen bonds with H_2O in the pore space. The maximum H_2O capacity reached 11.0 mmol·g^{-1} at a partial pressure ratio (p/p_0) of 0.92 and a temperature of 298 K, which is comparable to that of zeolite desiccants such as zeolite 4A (11.6 mmol·g^{-1}),[44] zeolite 4A (14.4 mmol·g^{-1}),[44] and other types of zeolites.[45,46] And we found that the saturated water vapor adsorption capacity of Melem slightly decreased at 308 K (Figure S2). Thermogravimetric−differential scanning calorimetry was employed to quantify the heat of adsorption (Q_{st}). The calculated H_2O Q_{st} values for Melem was 62.43 kJ·mol^{-1} (Figure S3), suggesting that the interaction between Melem and water was much higher than that of silica gel desiccants (43−50 kJ·mol^{-1}).[47] The thermal weight loss curves of Melem and Melem−H_2O were depicted in Figure 2c. Melem−H_2O lost 14% of its weight before reaching 150 °C, mostly due to water loss from its pores (environmental RH about 45%). In addition, we examined the impact of dehydration temperature on the dehydration efficiency of Melem−H_2O (Figure S4). Melem only lost 12% and 13% of its weight in 2 h at 70 and 90 °C, respectively. At 110 and 130 °C, Melem took 12 and 20 min, respectively, to lose all the water in the pores. Adsorption−desorption cycles of Melem revealed a full and rapid dehydration, which can be achieved after simple heating at 110 °C under vacuum. Additionally, Melem has demonstrated a strong recycling ability. After the 5-cycle water adsorption, there was no decline in H_2O uptake, and the structural integrity of reactivated HOF was still reserved (Figure 2d and Figure S5).

After achieving satisfactory H_2O adsorption and exhibiting excellent thermal stability, we tested the CO_2 and CH_4 adsorption and desorption isotherms for Melem to explore further the interaction between gases and the Melem structures. Melem can adsorb a small amount of CO_2 and CH_4 (Figure 2b). As for CO_2 adsorption, the observed CO_2 uptake at 1 atm reaches 1.07 cm^3·g^{-1} at 298 K, which increases

https://doi.org/10.1021/cbe.3c00114
Chem Bio Eng. 2024, 1, 283−288

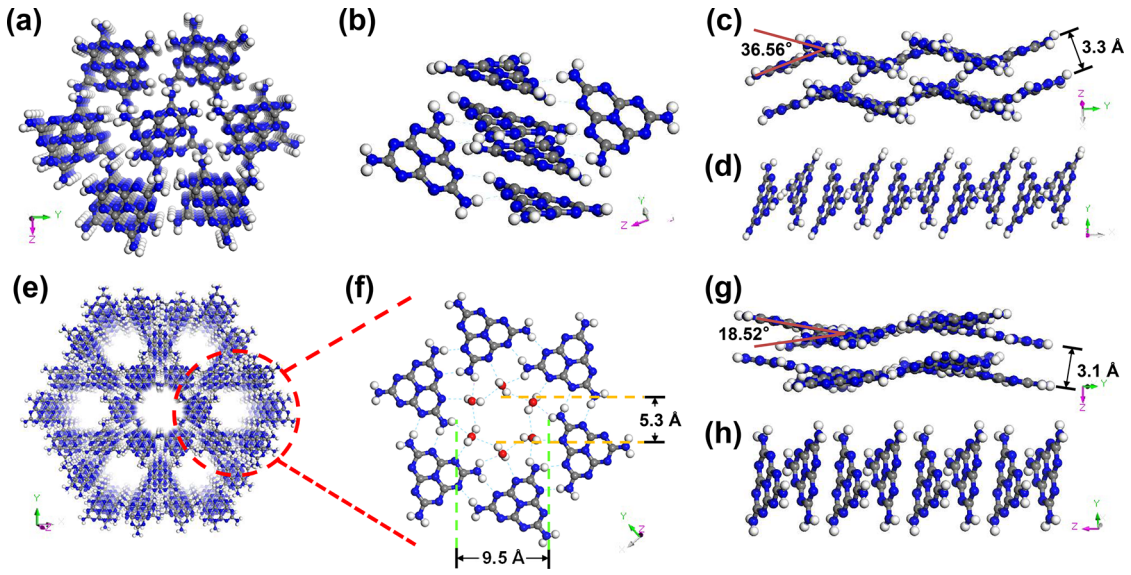

Figure 1. (a) The structure of Melem. (b) The hydrogen bonds in Melem. (c) The layer distance in Melem. (d) The stacked inversion CN heterocyclic rings in Melem. (e) The 1D channels of the Melem−H_2O (water molecule are omitted). (f) The water hexamers in Melem−H_2O. (g) The layer distance in Melem−H_2O. (h) The stacked inversion CN heterocyclic rings in Melem−H_2O. The red, white, gray, and blue balls represent O, H, C, and N atoms, respectively.

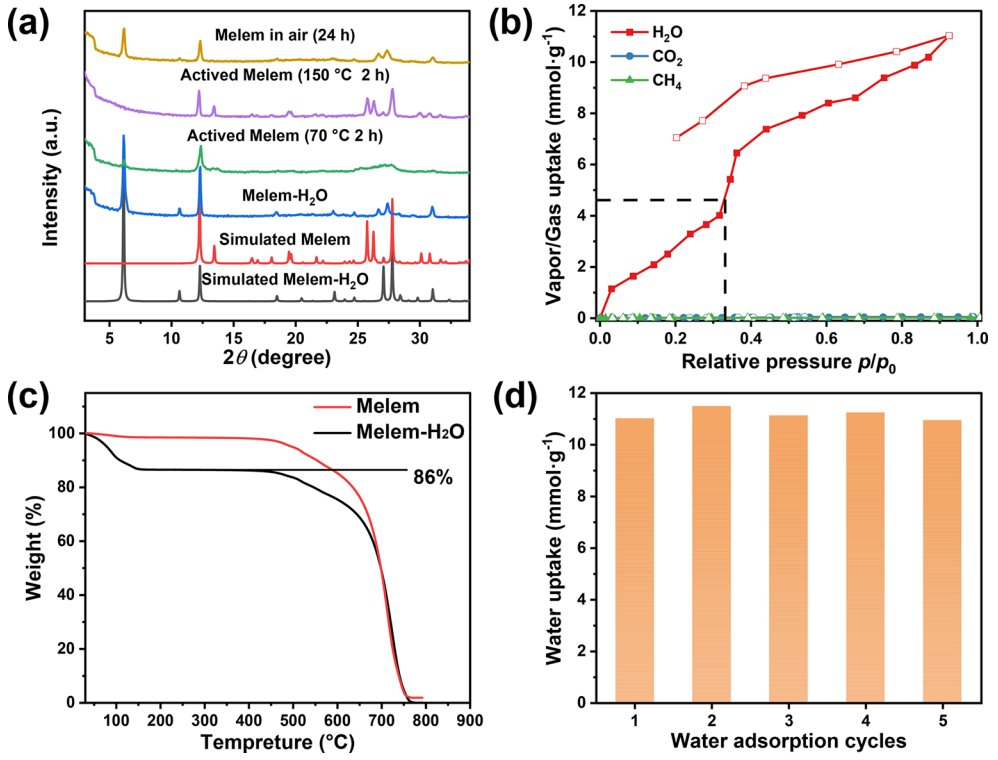

Figure 2. (a) The PXRD patterns of Melem and Melem−H_2O after treating with different conditions. (b) The adsorption isotherms of Melem for H_2O, CO_2, and CH_4 at 298 K. The solid symbols represent adsorption, while open symbols represent desorption. (c) The thermogravimetric analysis (TGA) curves of Melem and Melem−H_2O. (d) Adsorption cycles for Melem, adsorption at 298 K and desorption at 383 K.

to 1.75 $cm^3 \cdot g^{-1}$ at 273 K (Figure S6). According to the PXRD patterns of Melem before and after CO_2 adsorption, it is evident that Melem did not undergo a phase transition due to CO_2 (Figure S7). Solid desiccants often show highly competitive adsorption of H_2O and CO_2. To investigate the effect of water in pores on CO_2 adsorption performance, we tested the CO_2 adsorption curve of Melem−H_2O (Figure S8). The CO_2 adsorption capacities of Melem−H_2O are slightly higher than the uptakes of nonporous Melem. The H_2O molecules in the 1D pores do not increase the adsorption capacity of CO_2. As for CH_4 adsorption, the observed CH_4 uptake at 1 atm reaches 0.52 $cm^3 \cdot g^{-1}$ at 298 K, which increases to 0.57 $cm^3 \cdot g^{-1}$ at 273 K (Figure S9).

To elucidate the mechanism of H_2O selective adsorption in Melem and the structural transformation during H_2O adsorption, density functional theory (DFT) calculations

https://doi.org/10.1021/cbe.3c00114
Chem Bio Eng. 2024, 1, 283−288

were carried out. As shown in Figure 3a, the Melem molecule in Melem hydrogen-bonded to adjacent Melem molecules

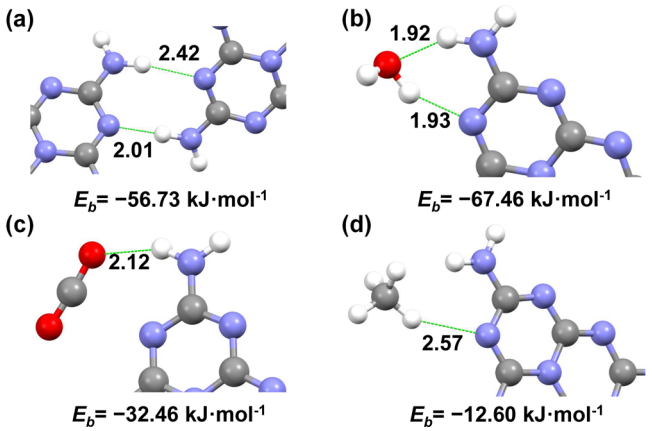

Figure 3. DFT-calculated binding energies and distances between (a) Melem molecules in Melem, (b) the Melem molecule and H_2O, (c) the Melem molecule and CO_2, and (d) the Melem molecule and CH_4. The unit for bond distance is Å. The red, white, gray, and blue balls represent O, H, C, and N atoms, respectively.

through the N atom and amino group, with a binding energy of −59.73 kJ·mol^{-1}. When the H_2O molecule was introduced into the system, the O atom of H_2O prioritized hydrogen-bonding with the amino group, while the H atom of H_2O hydrogen-bonded with the N atom, with a binding energy of −67.46 kJ·mol^{-1} (Figure 3b), sufficient to disrupt the hydrogen-bonded structure of Melem. The static H_2O binding energy derived from the DFT calculations was in good agreement with the value obtained from the vapor adsorption isotherms. Upon transformation into Melem−H_2O, the dihedral angle of the Melem molecules decreased to 18.52°, concurrent with an increase in binding energy to −87.23 kJ·mol^{-1} (Figure S10). This implies that the adsorbed water would not disrupt the hydrogen bonding network structure of Melem−H_2O. In contrast, the binding energies for CO_2 and CH_4 were significantly weaker, at −32.46 kJ·mol^{-1} and −12.60 kJ·mol^{-1}, respectively (Figure 3c,d), and were not adequate to break the original structure of the nonporous Melem and open up its pores.

The adsorption selectivity of Melem for H_2O indicates its potential as a gas desiccant. We evaluated adsorption competition between water in CH_4- and CO_2-containing gas streams, as would occur for separation involving natural gas and syngas of methane dry reforming. We performed breakthrough adsorption column experiments on H_2O vapor (single component) and in the presence of CH_4 and CO_2 using a similar total flow of 40 cm^3·min^{-1}. The data were analyzed by mass spectrometry, and the H_2O retention times in the column reached 95−105 min·g^{-1} at 20% RH (Figure S11). The retention time of H_2O in the column decreased as the RH increased (Figure S12). The presence of CH_4 or gas mixture (CO_2/CH_4: 50/50) did not affect the retention time of H_2O (Figure 4a,b). The separation factor was calculated to be about 654 according to the column breakthrough experiments. Melem could maintain stable retention time and obtain dried CH_4 for three consecutive breakthrough cycles (Figure S13). H_2O can be fully separated from gases, which confirms that Melem is a potential adsorbent capable of full discrimination of the water molecules in the gas by hydration/dehydration-induced reversible transformation mechanism.

In conclusion, we introduced a hydration/dehydration-induced reversible transformation approach and employed flexible Melem for targeted recognition and uptake of H_2O in gas dehydration. Structural transitions between Melem and Melem−H_2O can be observed during the water adsorption and desorption processes. Significantly, the nonporous structure confers upon Melem a minimal adsorption capacity for gases, thereby preventing the adsorption of gases by the dehydrant during the dehydration process. Melem has an adsorption capacity of 11.0 mmol·g^{-1} for water at 25 °C and can be regenerated to its original adsorption capacity at only 110 °C. Column breakthrough experiments demonstrated its effectiveness in drying gases. The separation factor was calculated to be about 654. Consequently, Melem has exhibited high selectivity and affinity for H_2O, rendering it an up-and-coming candidate for the effective dehydration of industrial gases.

■ ASSOCIATED CONTENT

Supporting Information

The Supporting Information is available free of charge at https://pubs.acs.org/doi/10.1021/cbe.3c00114.

Additional experimental details, chemicals, instrumentation, and materials characterization; crystal data; SEM images, gas/vapor adsorption analysis, TGA curves,

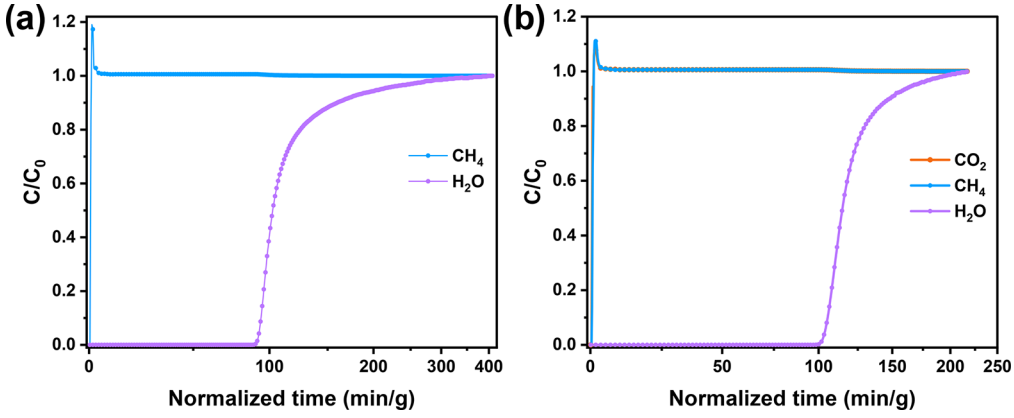

Figure 4. Column breakthrough experiments for (a) CH_4 (20% RH) and (b) CO_2/CH_4 mixture (50/50, 20% RH) with He as a carrier gas at 25 °C.

https://doi.org/10.1021/cbe.3c00114
Chem Bio Eng. 2024, 1, 283−288

PXRD, binding energies and distances, column breakthrough experiments, NMR and FTIR spectra (PDF)

AUTHOR INFORMATION

Corresponding Authors

Yunbo Bi − *Shanghai Key Laboratory of Molecular Catalysis and Innovative Materials, Department of Chemistry, Fudan University, Shanghai 200438, P. R. China*; Email: peiqimof2019@163.com

Peng Li − *Shanghai Key Laboratory of Molecular Catalysis and Innovative Materials, Department of Chemistry, Fudan University, Shanghai 200438, P. R. China*; orcid.org/0000-0002-4273-4577; Email: penglichem@fudan.edu.cn

Authors

Yao Wang − *Shanghai Key Laboratory of Molecular Catalysis and Innovative Materials, Department of Chemistry, Fudan University, Shanghai 200438, P. R. China*; orcid.org/0000-0002-0378-1805

Xiyu Song − *Shanghai Key Laboratory of Molecular Catalysis and Innovative Materials, Department of Chemistry, Fudan University, Shanghai 200438, P. R. China*; orcid.org/0000-0002-0208-8259

Guanglai Mo − *Shanghai Key Laboratory of Molecular Catalysis and Innovative Materials, Department of Chemistry, Fudan University, Shanghai 200438, P. R. China*

Xiangyu Gao − *Shanghai Key Laboratory of Molecular Catalysis and Innovative Materials, Department of Chemistry, Fudan University, Shanghai 200438, P. R. China*

Enyu Wu − *State Key Laboratory of Silicon Materials, School of Materials Science and Engineering, Zhejiang University, Hang-zhou 310027, China*

Bin Li − *State Key Laboratory of Silicon Materials, School of Materials Science and Engineering, Zhejiang University, Hang-zhou 310027, China*; orcid.org/0000-0002-7774-5452

Complete contact information is available at: https://pubs.acs.org/10.1021/cbe.3c00114

Author Contributions

Y.W., X.S., G.M., X.G., and E.W. conducted most of the experiments and collected the data; Y.W. and X.S. analyzed the data; Y.W. and P.L. conceived and designed the experiments; Y.W. wrote the manuscript; P.L., Y.B., and B.L. provided project administration, resources, and supervision.

Notes

The authors declare no competing financial interest.

ACKNOWLEDGMENTS

P.L. gratefully acknowledges the financial support from the start-up fund of Fudan University and the fund of the State Key Laboratory for Modification of Chemical Fibers and Polymer Materials, Donghua University (KF2103).

REFERENCES

(1) Liu, Z.; Li, Y.; Wang, W.; Song, G.; Ning, Y.; Liu, X.; Zhang, J. Investigation into the formation, blockage and dissociation of cyclopentane hydrate in a visual flow loop. *Fuel* **2022**, *307*, 121730−121746.

(2) Liu, E.-B.; Tang, H.; Zhang, Y.-H.; Li, D.-J.; Kou, B.; Liu, N.; Azimi, M. Experiment and numerical simulation of distribution law of water-based corrosion inhibitor in natural gas gathering and transportation pipeline. *Petroleum Science* **2023**, *20*, 1857−1873.

(3) Buelens, L. C.; Galvita, V. V.; Poelman, H.; Detavernier, C.; Marin, G. B. Super-dry reforming of methane intensifies CO_2 utilization via Le Chatelier's principle. *Science* **2016**, *354*, 449−452.

(4) Wynnyk, K. G.; Hojjati, B.; Marriott, R. A. Sour Gas and Water Adsorption on Common High-Pressure Desiccant Materials: Zeolite 3A, Zeolite 4A, and Silica Gel. *J. Chem. Eng. Data* **2019**, *64*, 3156−3163.

(5) Kitagawa, S.; Kitaura, R.; Noro, S.-i. Functional Porous Coordination Polymers. *Angew. Chem. Int. Ed.* **2004**, *43*, 2334−2375.

(6) Cadiau, A.; Belmabkhout, Y.; Adil, K.; Bhatt, P. M.; Pillai, R. S.; Shkurenko, A.; Martineau-Corcos, C.; Maurin, G.; Eddaoudi, M. Hydrolytically stable fluorinated metal-organic frameworks for energy-efficient dehydration. *Science* **2017**, *356*, 731−735.

(7) Zhang, L.; Fang, W.-X.; Wang, C.; Dong, H.; Ma, S.-H.; Luo, Y.-H. Porous frameworks for effective water adsorption: from 3D bulk to 2D nanosheets. *Inorg. Chem. Front.* **2021**, *8*, 898−913.

(8) Zu, K.; Qin, M.; Cui, S. Progress and potential of metal-organic frameworks (MOFs) as novel desiccants for built environment control: A review. *Renew. Sust. Energy Rev.* **2020**, *133*, 110246−110264.

(9) Wang, Y.; Chang, J.-P.; Xu, R.; Bai, S.; Wang, D.; Yang, G.-P.; Sun, L.-Y.; Li, P.; Han, Y.-F. N-Heterocyclic carbenes and their precursors in functionalised porous materials. *Chem. Soc. Rev.* **2021**, *50*, 13559−13586.

(10) Li, L.; Guo, L.; Olson, D. H.; Xian, S.; Zhang, Z.; Yang, Q.; Wu, K.; Yang, Y.; Bao, Z.; Ren, Q.; Li, J. Discrimination of xylene isomers in a stacked coordination polymer. *Science* **2022**, *377*, 335−339.

(11) Reynolds, J. E.; Bohnsack, A. M.; Kristek, D. J.; Gutiérrez-Alejandre, A.; Dunning, S. G.; Waggoner, N. W.; Sikma, R. E.; Ibarra, I. A.; Humphrey, S. M. Phosphonium zwitterions for lighter and chemically-robust MOFs: highly reversible H_2S capture and solvent-triggered release. *J. Mater. Chem. A* **2019**, *7*, 16842−16849.

(12) Poschmann, M. P. M.; Alan, Ö.; Ito, S.; Näther, C.; Friedrichs, G.; Stock, N. Systematic Study on Zirconium Chelidamates: From a Molecular Complex to a M-HOF and a MOF. *Inorg. Chem.* **2023**, *62*, 12252−12259.

(13) Zhang, T.; Lin, S.; Yan, T.; Li, B.; Liang, Y.; Liu, D.; He, Y. Integrating Self-Partitioned Pore Space and Amine Functionality into an Aromatic-Rich Coordination Framework with Ph Stability for Effective Purification of C2 Hydrocarbons. *Inorg. Chem.* **2023**, *62*, 5593−5601.

(14) Soleimani Abhari, P.; Gholizadeh, S.; Rouhani, F.; Li, Y.-L.; Morsali, A.; Liu, T.-F. Recent progress in gas separation platforms based on hydrogen-bonded organic frameworks (HOFs). *Inorg. Chem. Front.* **2023**, *10*, 6134−6159.

(15) Song, X.; Wang, Y.; Wang, C.; Wang, D.; Zhuang, G.; Kirlikovali, K. O.; Li, P.; Farha, O. K. Design Rules of Hydrogen-Bonded Organic Frameworks with High Chemical and Thermal Stabilities. *J. Am. Chem. Soc.* **2022**, *144*, 10663−10687.

(16) Ma, L.; Xie, Y.; Khoo, R. S. H.; Arman, H.; Wang, B.; Zhou, W.; Zhang, J.; Lin, R. B.; Chen, B. An Adaptive Hydrogen Bonded Organic Framework for the Exclusive Recognition of *p* Xylene. *Chem.—Eur. J.* **2022**, *28*, e202104269.

(17) Chen, L.; Yuan, Z.; Zhang, H.; Ye, Y.; Yang, Y.; Xiang, F.; Cai, K.; Xiang, S.; Chen, B.; Zhang, Z. A Flexible Hydrogen Bonded Organic Framework Constructed from a Tetrabenzaldehyde with a Carbazole N-H Binding Site for the Highly Selective Recognition and Separation of Acetone. *Angew. Chem. Int. Ed.* **2022**, *61*, e202213959.

(18) Yu Gao, X.; Wang, Y.; Wu, E.; Wang, C.; Li, B.; Zhou, Y.; Chen, B.; Li, P. Multivariate Hydrogen-Bonded Organic Frameworks with Tunable Permanent Porosities for Capture of a Mustard Gas Simulant. *Angew. Chem. Int. Ed.* **2023**, *62*, e202312393.

(19) Xing, G.; Yan, T.; Das, S.; Ben, T.; Qiu, S. Synthesis of Crystalline Porous Organic Salts with High Proton Conductivity. *Angew. Chem. Int. Ed.* **2018**, *57*, 5345−5349.

(20) Yang, Z.; Zhang, Y.; Wu, W.; Zhou, Z.; Gao, H.; Wang, J.; Jiang, Z. Hydrogen-bonded organic framework membrane with efficient proton conduction. *J. Membr. Sci.* **2022**, *664*, 121118.

(21) Wang, B.; He, R.; Xie, L.-H.; Lin, Z.-J.; Zhang, X.; Wang, J.; Huang, H.; Zhang, Z.; Schanze, K. S.; Zhang, J.; Xiang, S.; Chen, B. Microporous Hydrogen-Bonded Organic Framework for Highly Efficient Turn-Up Fluorescent Sensing of Aniline. *J. Am. Chem. Soc.* **2020**, *142*, 12478−12485.
(22) Wang, Y.; Liu, D.; Yin, J.; Shang, Y.; Du, J.; Kang, Z.; Wang, R.; Chen, Y.; Sun, D.; Jiang, J. An ultrafast responsive NO_2 gas sensor based on a hydrogen-bonded organic framework material. *Chem. Commun.* **2020**, *56*, 703−706.
(23) Wang, C.; Wang, Y.; Kirlikovali, K. O.; Ma, K.; Zhou, Y.; Li, P.; Farha, O. K. Ultrafine Silver Nanoparticle Encapsulated Porous Molecular Traps for Discriminative Photoelectrochemical Detection of Mustard Gas Simulants by Synergistic Size-Exclusion and Site-Specific Recognition. *Adv. Mater.* **2022**, *34*, 2202287.
(24) Wang, C.; Song, X.; Wang, Y.; Xu, R.; Gao, X.; Shang, C.; Lei, P.; Zeng, Q.; Zhou, Y.; Chen, B.; Li, P. A Solution-Processable Porphyrin-Based Hydrogen-Bonded Organic Framework for Photoelectrochemical Sensing of Carbon Dioxide. *Angew. Chem. Int. Ed.* **2023**, *62*, e202311482.
(25) Chen, G.; Tong, L.; Huang, S.; Huang, S.; Zhu, F.; Ouyang, G. Hydrogen-bonded organic framework biomimetic entrapment allowing non-native biocatalytic activity in enzyme. *Nat. Commun.* **2022**, *13*, 4816−4825.
(26) Liang, W.; Carraro, F.; Solomon, M. B.; Bell, S. G.; Amenitsch, H.; Sumby, C. J.; White, N. G.; Falcaro, P.; Doonan, C. J. Enzyme Encapsulation in a Porous Hydrogen-Bonded Organic Framework. *J. Am. Chem. Soc.* **2019**, *141*, 14298−14305.
(27) Liu, S.; Sun, Y. Co-encapsulating Cofactor and Enzymes in Hydrogen-Bonded Organic Frameworks for Multienzyme Cascade Reactions with Cofactor Recycling. *Angew. Chem. Int. Ed.* **2023**, *62*, e202308562.
(28) Wang, Y.; Cao, R.; Wang, C.; Song, X.; Wang, R.; Liu, J.; Zhang, M.; Huang, J.; You, T.; Zhang, Y.; Yan, D.; Han, W.; Yan, L.; Xiao, J.; Li, P. In Situ Embedding Hydrogen-Bonded Organic Frameworks Nanocrystals in Electrospinning Nanofibers for Ultrastable Broad-Spectrum Antibacterial Activity. *Adv. Funct. Mater.* **2023**, *33*, 2214388.
(29) Wang, Y.; Ma, K.; Bai, J.; Xu, T.; Han, W.; Wang, C.; Chen, Z.; Kirlikovali, K. O.; Li, P.; Xiao, J.; Farha, O. K. Chemically Engineered Porous Molecular Coatings as Reactive Oxygen Species Generators and Reservoirs for Long-Lasting Self-Cleaning Textiles. *Angew. Chem. Int. Ed.* **2022**, *61*, e202115956.
(30) Yu, D.; Zhang, H.; Ren, J.; Qu, X. Hydrogen-bonded organic frameworks: new horizons in biomedical applications. *Chem. Soc. Rev.* **2023**, *52*, 7504−7523.
(31) Huang, W.; Yuan, H.; Yang, H.; Tong, L.; Gao, R.; Kou, X.; Wang, J.; Ma, X.; Huang, S.; Zhu, F.; Chen, G.; Ouyang, G. Photodynamic Hydrogen-Bonded Biohybrid Framework: A Photobiocatalytic Cascade Nanoreactor for Accelerating Diabetic Wound Therapy. *JACS Au* **2022**, *2*, 2048−2058.
(32) Gao, X.; Lu, W.; Wang, Y.; Song, X.; Wang, C.; Kirlikovali, K. O.; Li, P. Recent advancements of photo- and electro-active hydrogen-bonded organic frameworks. *Science China Chemistry* **2022**, *65*, 2077−2095.
(33) Huang, Q.; Li, W.; Mao, Z.; Qu, L.; Li, Y.; Zhang, H.; Yu, T.; Yang, Z.; Zhao, J.; Zhang, Y.; Aldred, M. P.; Chi, Z. An exceptionally flexible hydrogen-bonded organic framework with large-scale void regulation and adaptive guest accommodation abilities. *Nat. Commun.* **2019**, *10*, 3074−3081.
(34) Song, X.; Wang, Y.; Wang, C.; Gao, X.; Zhou, Y.; Chen, B.; Li, P. Self-Healing Hydrogen-Bonded Organic Frameworks for Low-Concentration Ammonia Capture. *J. Am. Chem. Soc.* **2024**, *146*, 627−634.
(35) Rahmani, M.; Matos, C. R. M. O.; Wang, S.-Q.; Bezrukov, A. A.; Eaby, A. C.; Sensharma, D.; Hjiej-Andaloussi, Y.; Vandichel, M.; Zaworotko, M. J. Highly Selective *p*-Xylene Separation from Mixtures of C8 Aromatics by a Nonporous Molecular Apohost. *J. Am. Chem. Soc.* **2023**, *145*, 27316.
(36) Kenfack Tsobnang, P.; Sakam Nchedoung, Y. T.; Fröhlich, D.; Porcher, F.; Rustam, L.; Hastürk, E.; Janiak, C. Structural transitions during the water sorption process in two layered metal hydrogen-bonded organic frameworks and the effect of the H-bond strength between the layers. *CrystEngComm* **2022**, *24*, 3338−3346.
(37) Luo, Y. H.; He, X. T.; Hong, D. L.; Chen, C.; Chen, F. H.; Jiao, J.; Zhai, L. H.; Guo, L. H.; Sun, B. W. A Dynamic 3D Hydrogen Bonded Organic Frameworks with Highly Water Affinity. *Adv. Funct. Mater.* **2018**, *28*, 1804822.
(38) Song, X.; Wang, C.; Gao, X.; Wang, Y.; Xu, R.; Wang, J.; Li, P. Thermally Crosslinked Hydrogen-Bonded Organic Framework Membranes for Highly Selective Ion Separation. *Molecules* **2023**, *28*, 2173.
(39) Jürgens, B.; Irran, E.; Senker, J.; Kroll, P.; Müller, H.; Schnick, W. Journal of the American Chemical SocietyMelem (2,5,8-Triamino-tri-s-triazine), an Important Intermediate during Condensation of Melamine Rings to Graphitic Carbon Nitride: Synthesis, Structure Determination by X-ray Powder Diffractometry, Solid-State NMR, and Theoretical Studies. *J. Am. Chem. Soc.* **2003**, *125*, 10288−10300.
(40) Lei, R.; Du, B.; Lai, X.; Wu, J.; Zhang, Z.; Liu, S.; Wu, R.; Li, X.; Song, B.; Jian, J. Single-crystalline Melem ($C_6N_{10}H_6$) nanorods: a novel stable molecular crystal photocatalyst with modulated charge potentials and dynamics. *J. Mater. Chem. A* **2019**, *7*, 13234−13241.
(41) Sattler, A.; Schnick, W. Zur Kenntnis der Kristallstruktur von Melem $C_6N_7(NH_2)_3$. *Z. Anorg. Allg. Chem.* **2006**, *632*, 238−242.
(42) Makowski, S. J.; Köstler, P.; Schnick, W. Formation of a Hydrogen Bonded Heptazine Framework by Self Assembly of Melem into a Hexagonal Channel Structure. *Chem.—Eur. J.* **2012**, *18*, 3248−3257.
(43) Dai, T.; Kiuchi, H.; Minamide, H.; Miyake, Y.; Inoki, H.; Sonoda, Y.; Tsutsumi, J. y.; Kanai, K. Growth and characterization of Melem hydrate crystals with a hydrogen-bonded heptazine framework. *Phys. Chem. Chem. Phys.* **2022**, *24*, 13922−13934.
(44) Volavšek, J.; Pliekhov, O.; Pliekhova, O.; Mali, G.; Zabukovec Logar, N. Study of Water Adsorption on EDTA-Modified LTA Zeolites. *Nanomaterials* **2022**, *12*, 1352.
(45) Tatlier, M.; Munz, G.; Henninger, S. K. Relation of water adsorption capacities of zeolites with their structural properties. *Microporous Mesoporous Mater.* **2018**, *264*, 70−75.
(46) Kraus, M.; Trommler, U.; Holzer, F.; Kopinke, F.-D.; Roland, U. Competing adsorption of toluene and water on various zeolites. *Chem. Eng. J.* **2018**, *351*, 356−363.
(47) Zhang, L.-Z.; Fu, H.-X.; Yang, Q.-R.; Xu, J.-C. Performance comparisons of honeycomb-type adsorbent beds (wheels) for air dehumidification with various desiccant wall materials. *Energy* **2014**, *65*, 430−440.

https://doi.org/10.1021/cbe.3c00114
Chem Bio Eng. 2024, 1, 283−288